Electronic Supplementary Material (ESI) for RSC Advances.

Supporting information

Influence of ZIF-9 and ZIF-12 structure on the formation of a series of new Co/N-doped porous carbon composites as anode electrodes for high-performance lithium-ion batteries

Anh T. A. Duong,[a] Hoang V. Nguyen,[b,c] Man V. Tran,[b,c] Quynh N. Ngo,[a] Loc C. Luu,[d] Tan L. H. Doan,[e,f] Hung N. Nguyen[a] and My V. Nguyen*[,a]

[a]Faculty of Chemistry, Ho Chi Minh City University of Education, Ho Chi Minh City 700000, Vietnam.

[b]Applied Physical Chemistry Laboratory (APCLAB), VNUHCM-University of Science, Ho Chi Minh City 700000, Vietnam.

[c]Department of Physical Chemistry, Faculty of Chemistry, VNUHCM-University of Science, Ho Chi Minh City 700000, Vietnam.

[d]HCMC University of Technology, VNU-HCM, 268 Ly Thuong Kiet, District 10, Ho Chi Minh City, Vietnam.

[e]Center for Innovative Materials and Architectures (INOMAR), Ho Chi Minh City, Viet Nam.

[f]Vietnam National University, Ho Chi Minh City, Vietnam.

*To whom correspondence should be addressed: mynv@hcmue.edu.vn

Table of Contents

Section S1	*Fourier Transform Infrared Spectroscopy (FT-IR)*	**S3-S4**
Section S2	*Thermogravimetric analysis (TGA) and Differential scanning calorimetry (DSC) curves*	**S5-S6**
Section S3	*N_2 adsorption-desorption measurement of Co/CZIF-9 and Co/CZIF-12 materials*	**S7-S9**
Section S4	*Energy-dispersive X-ray mapping (EDX-mapping) and transmission electron microscopy (TEM) analysis*	**S10-S12**
Section S5	*The electrochemical measurements of Co/CZIF-9 and Co/CZIF-12 materials*	**S13-S20**

Section S1. Fourier Transform Infrared Spectroscopy (FT-IR)

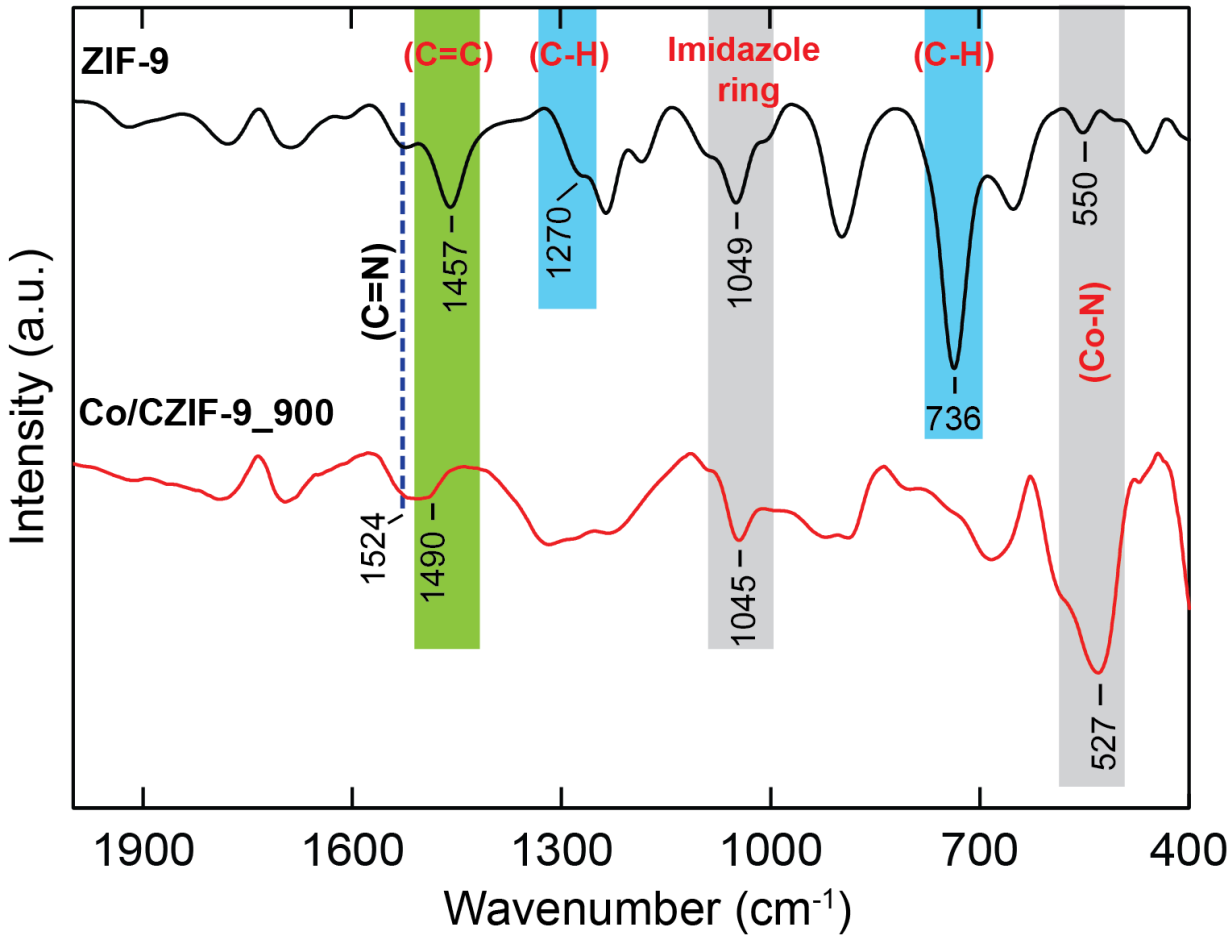

Figure S1. FT-IR spectra of activated ZIF-9 (black) in comparison with Co/CZIF-9_900 (red).

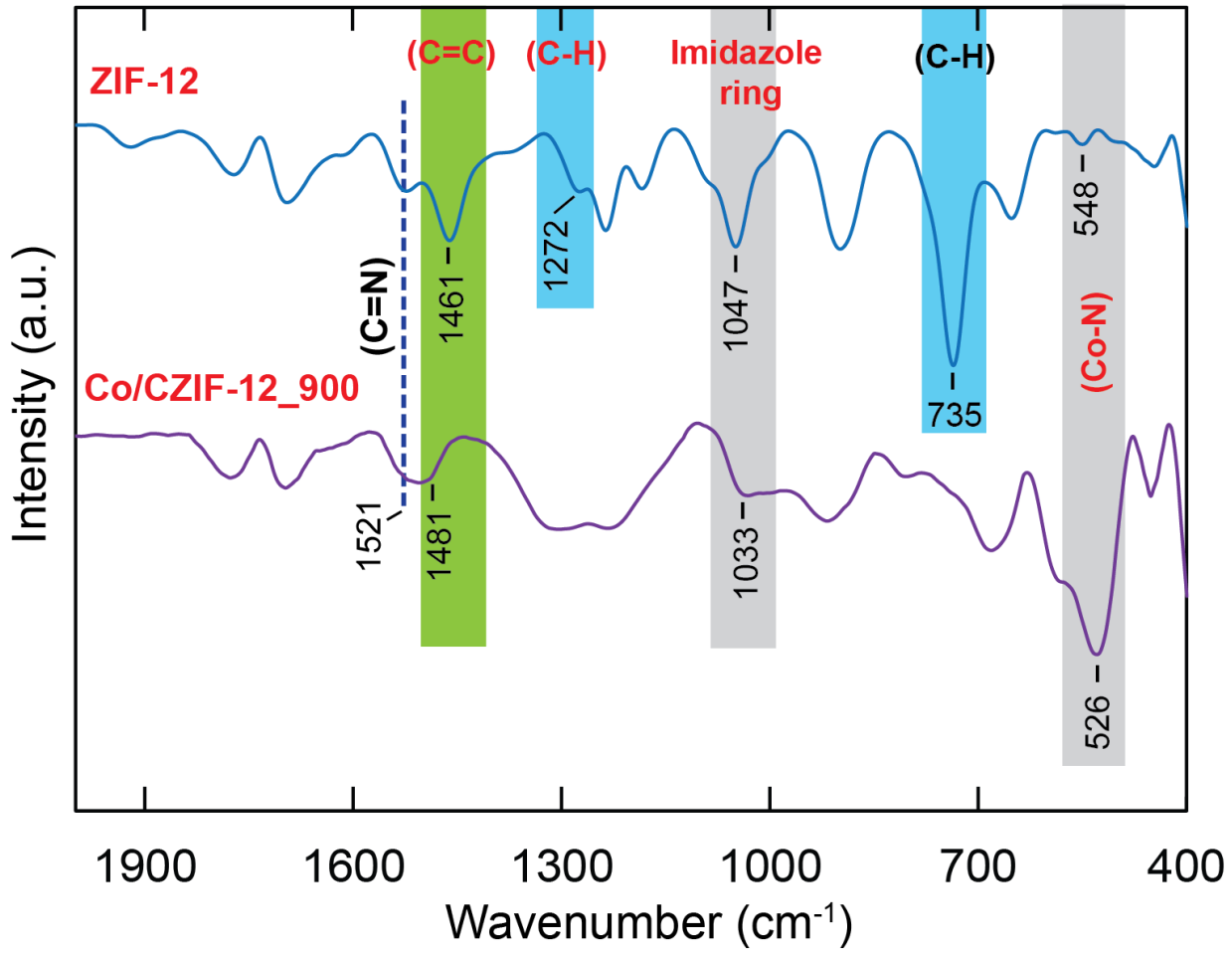

Figure S2. FT-IR spectra of activated ZIF-12 (blue) in comparison with Co/CZIF-12_900 (purple).

Section S2. Thermogravimetric analysis (TGA) and Differential scanning calorimetry (DSC) curves

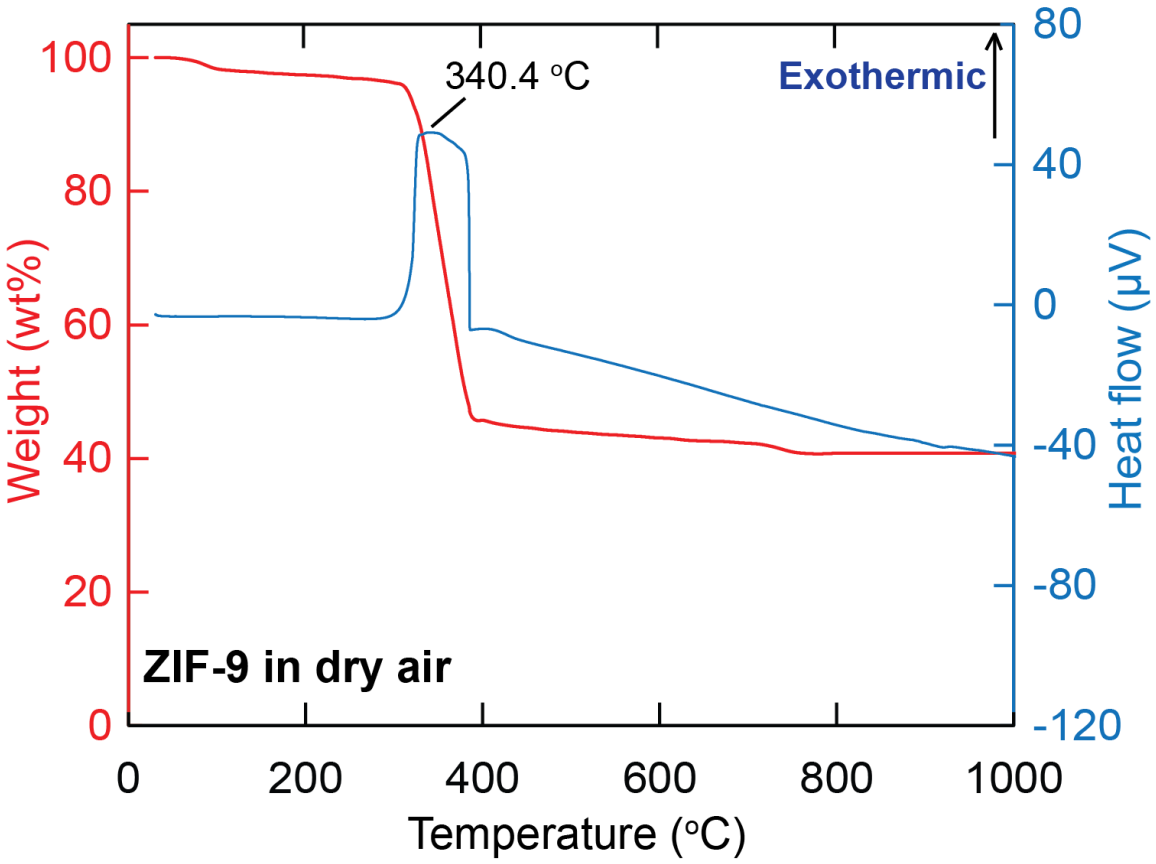

Figure S3. TGA-DSC curve of the activated ZIF-9 annealed in dry air. Herein, we further performed thermogravimetric analysis combined with differential scanning calorimetry (TGA-DSC) for ZIF-9 under dry air (80% N_2, 20% O_2). Specifically, the framework of ZIF-9 is confirmed to be thermally stable > 320 °C with a specific exothermic peak at 340.4 °C.

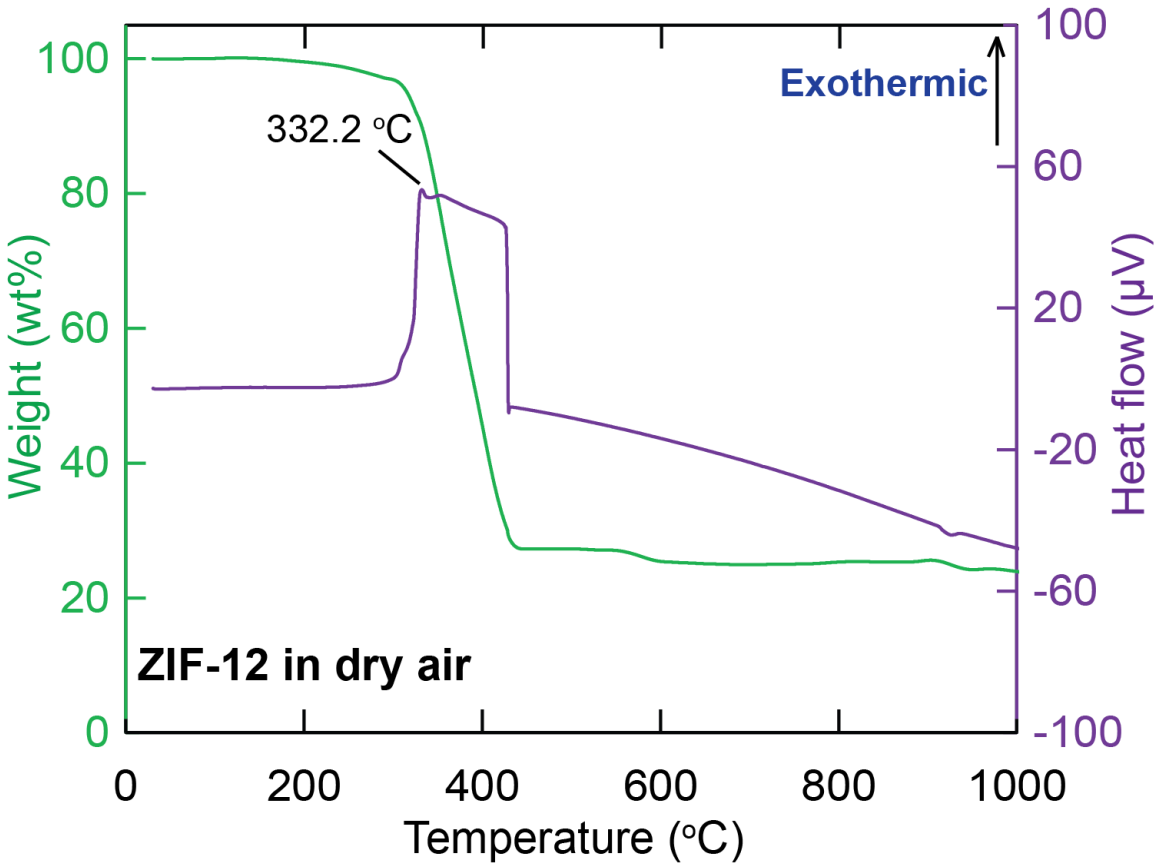

Figure S4. TGA-DSC curve of the activated ZIF-12 annealed in dry air. Herein, we further performed thermogravimetric analysis combined with differential scanning calorimetry (TGA-DSC) for ZIF-12 under dry air (80% N_2, 20% O_2). In detail, the framework of ZIF-12 is confirmed to be thermally stable > 320 °C with a specific exothermic peak at 332.2 °C.

Section S3. N_2 adsorption-desorption measurement of Co/CZIF-9 and Co/CZIF-12 materials

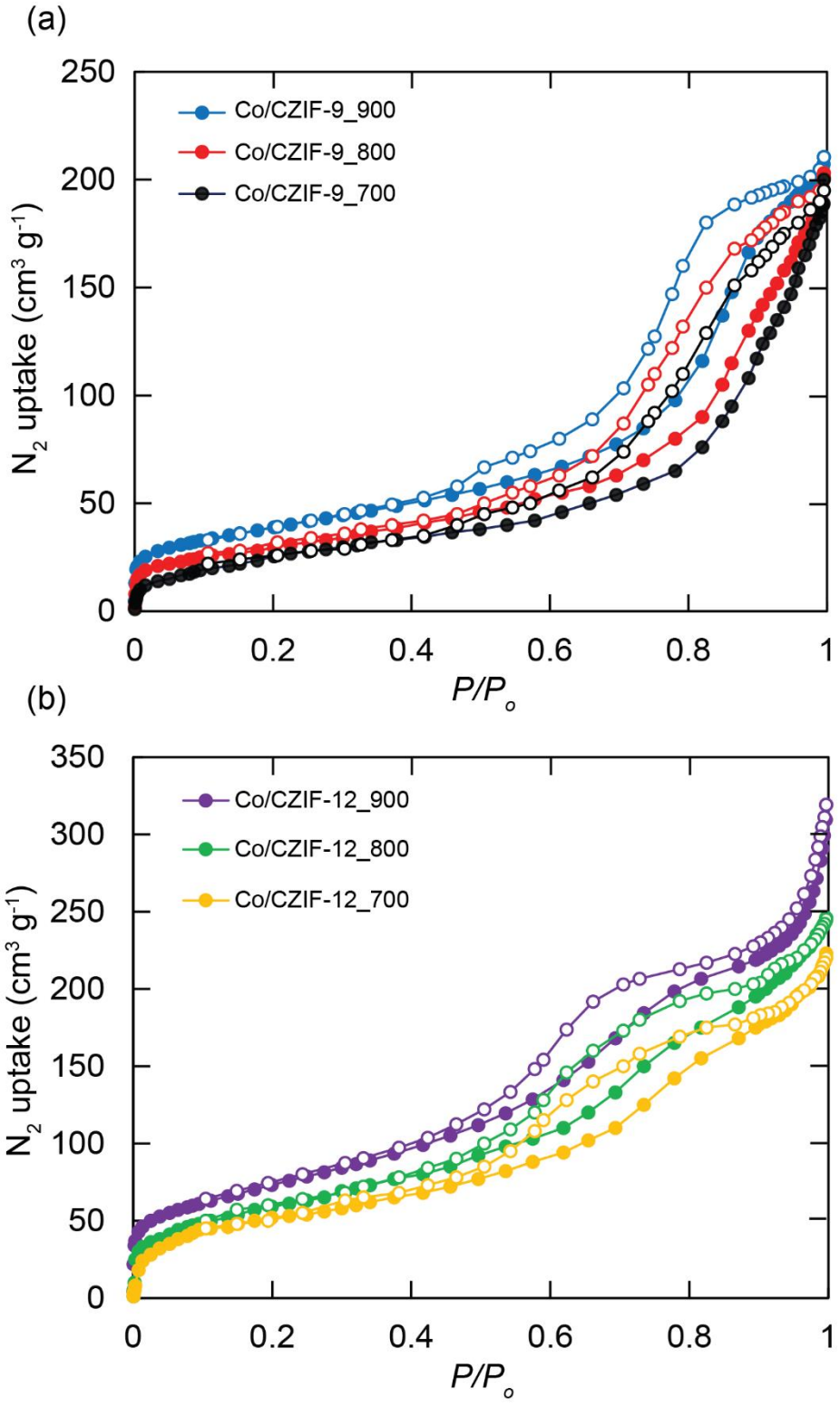

Figure S5. N_2 adsorption-desorption isotherm of Co/CZIF-9 (a) and Co/CZIF-12 (b) annealed at 700, 800, and 900 ^oC

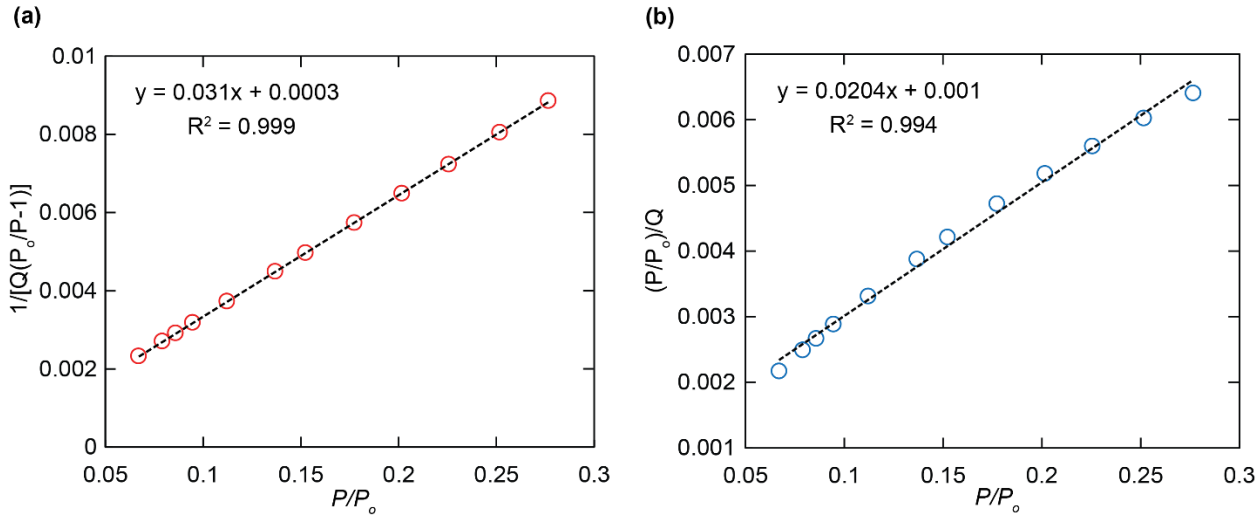

(c)

Parameters	**BET model**	**Langmuir model**
P/P_o range	0.067 - 0.277	0.067 - 0.277
Correlation Coefficient	0.999	0.994
C	123.28	20.40
Q_m ($cm^3\ g^{-1}$ STP)	31.974	49.020
Molecular cross-sectional area (S / nm^2)	0.1620	0.1620
Surface area ($m^2\ g^{-1}$)	139.17	213.42

$$S = \frac{Q_m \times N_A \times A}{V}$$

Where S and Q_m are the BET or Langmuir surface area and quantity adsorbed. N_A is Avogrado's number, A is the molecular-sectional area and V symbolizes the molar volume of adsorbed gas.

Figure S6. Plot of the linear region of the adsorption N_2 isotherm of Co/CZIF-9_900 used for the BET equation (a), the Langmuir equation (b), and summary of parameters in the BET and Langmuir analysis (c).

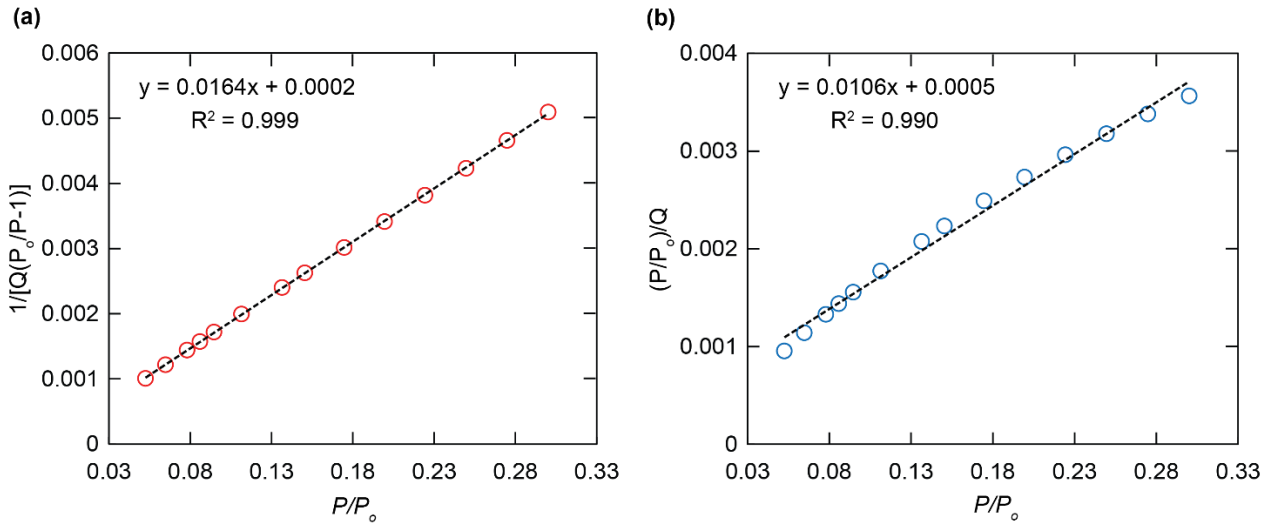

(c)

Parameters	**BET model**	**Langmuir model**
P/P_o range	0.053 - 0.300	0.053 - 0.300
Correlation Coefficient	0.999	0.990
C	103.30	21.20
Q_m ($cm^3\ g^{-1}$ STP)	60.532	94.340
Molecular cross-sectional area (S / nm^2)	0.1620	0.1620
Surface area ($m^2\ g^{-1}$)	263.47	410.73

$$S = \frac{Q_m \times N_A \times A}{V}$$

Where S and Q_m are the BET or Langmuir surface area and quantity adsorbed. N_A is Avogrado's number, A is the molecular-sectional area and V symbolizes the molar volume of adsorbed gas.

Figure S7. Plot of the linear region of the adsorption N_2 isotherm of Co/CZIF-12_900 used for the BET equation (a), the Langmuir equation (b), and summary of parameters in the BET and Langmuir analysis (c).

Section S4. Energy-dispersive X-ray mapping (EDX-mapping) and transmission electron microscopy (TEM) analysis

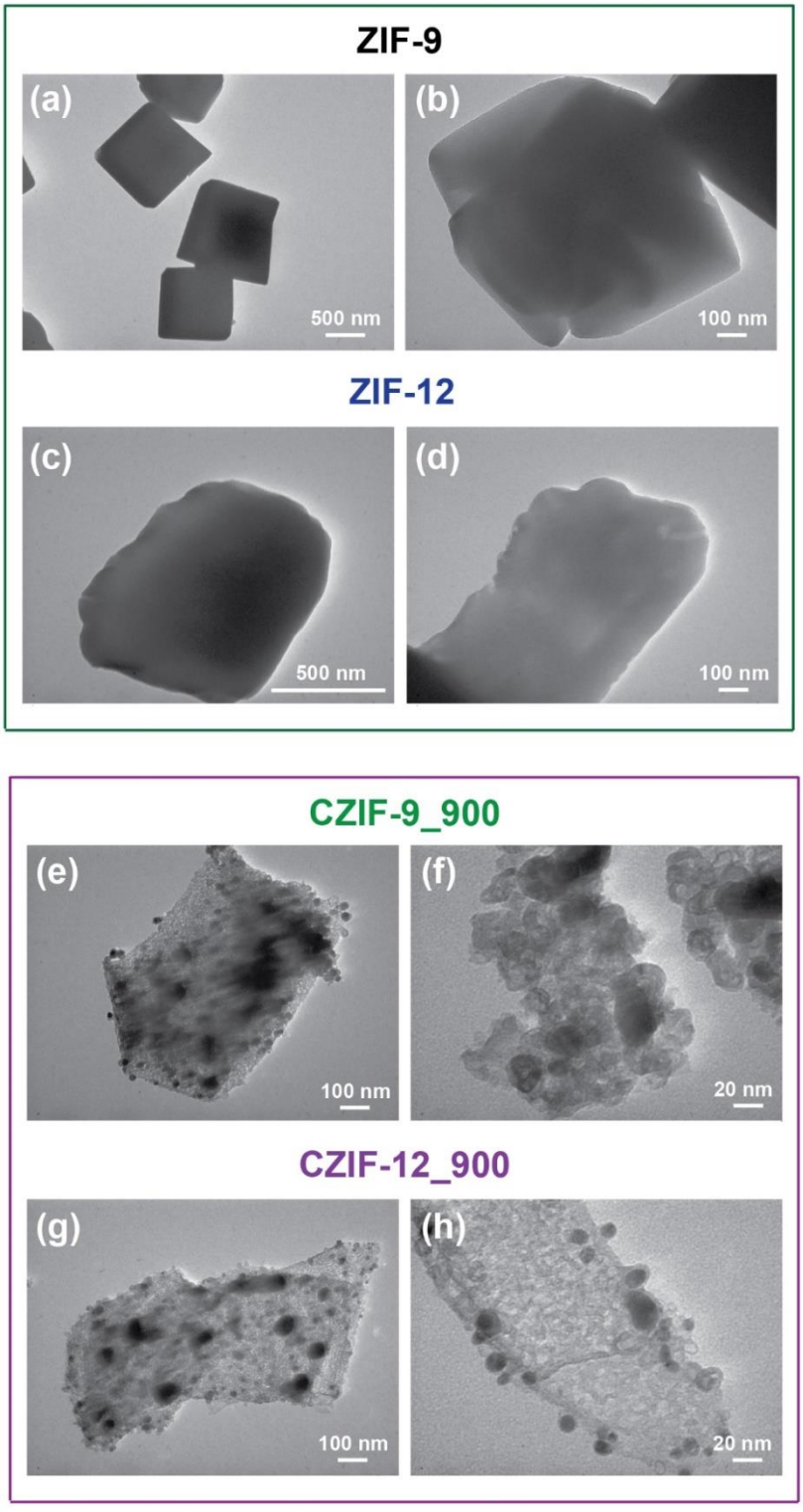

Figure S8. TEM images of ZIF-9 (a and b), ZIF-12 (c and d), Co/CZIF-9_900 (e and f), and Co/CZIF-12_900 (g and h).

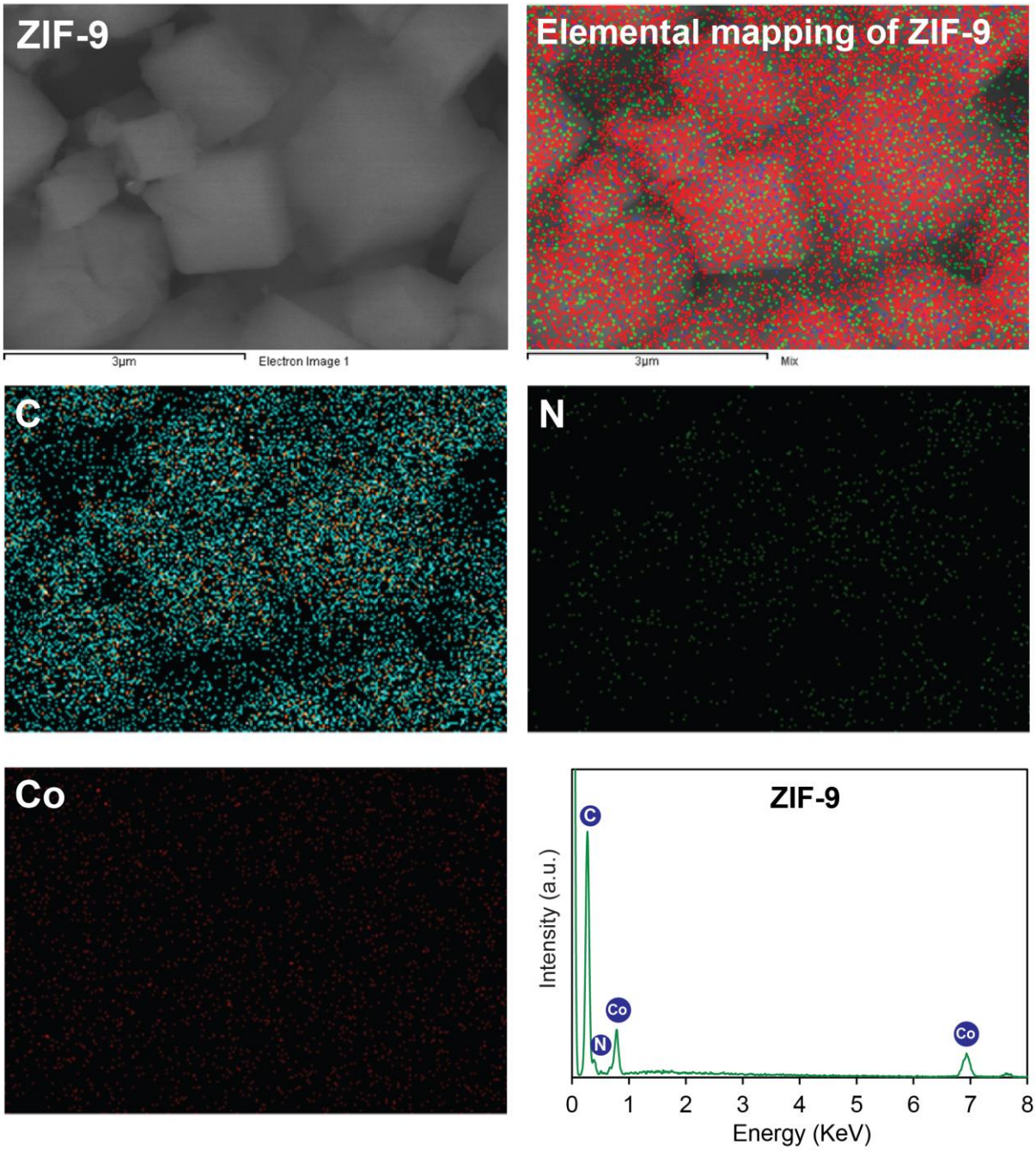

Figure S9. Elemental mapping by SEM-EDX of ZIF-9.

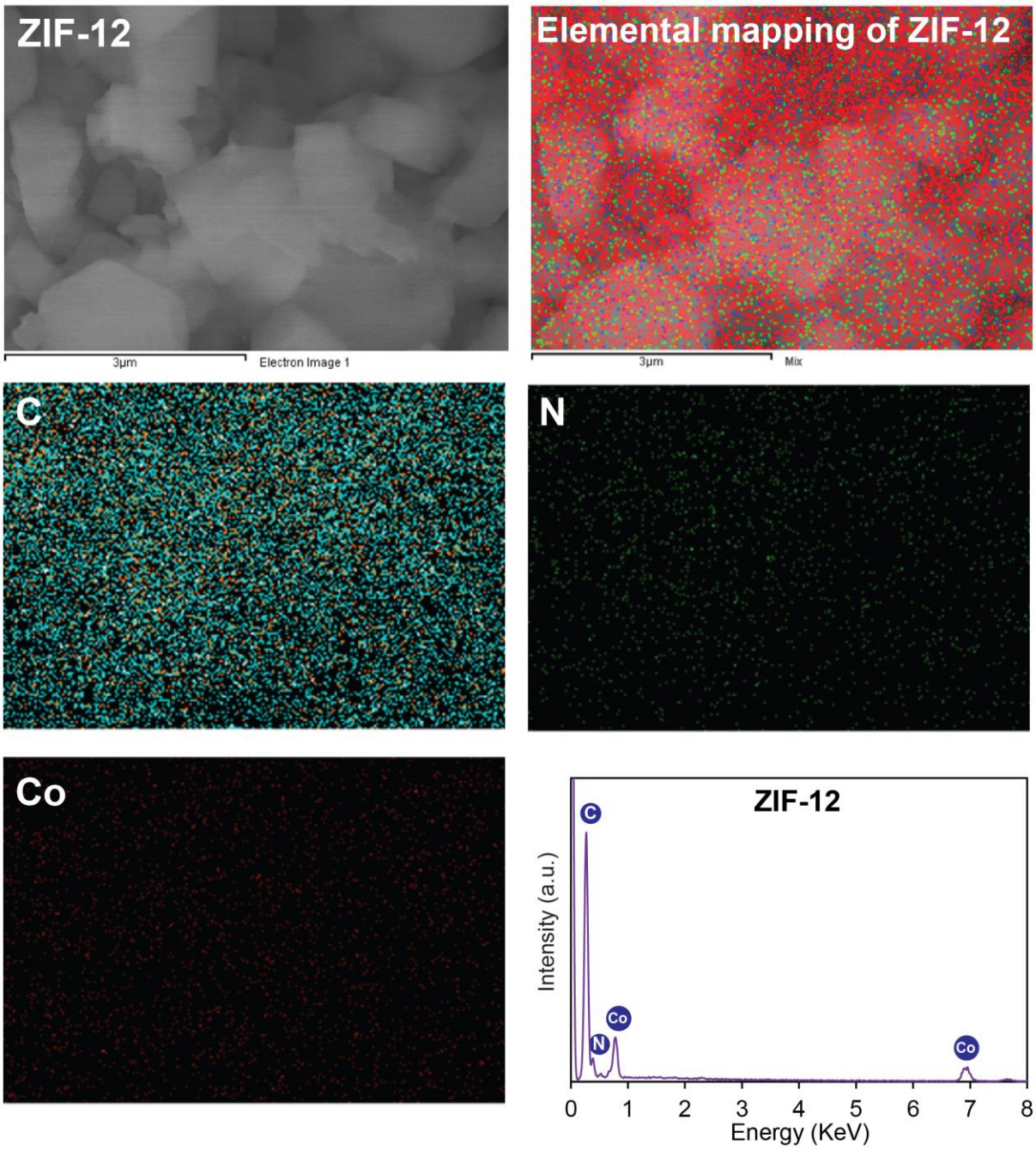

Figure S10. Elemental mapping by SEM-EDX of ZIF-12.

Section S5. The electrochemical measurements of Co/CZIF-9 and Co/CZIF-12 materials

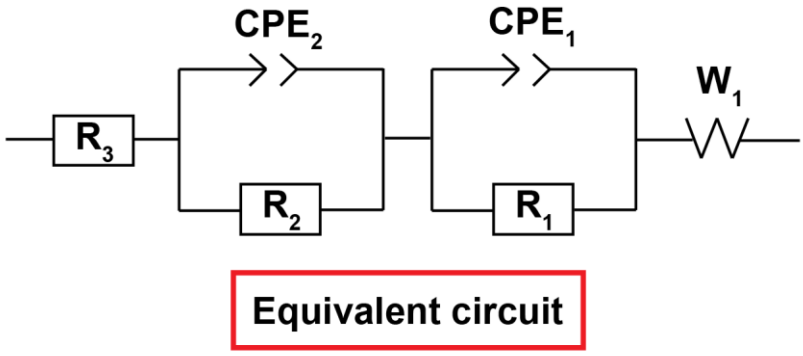

Figure S11. An equivalent circuit used for fitting. Schematic representations: $R_1/R_2/R_3$, the resistance of charge transfer, the resistor of the SEI film and the internal resistor of the battery; CPE_1/CPE_2, the constant phase element of the electrode/electrolyte interface and the SEI layer; W_1, Warburg diffusion element**.**

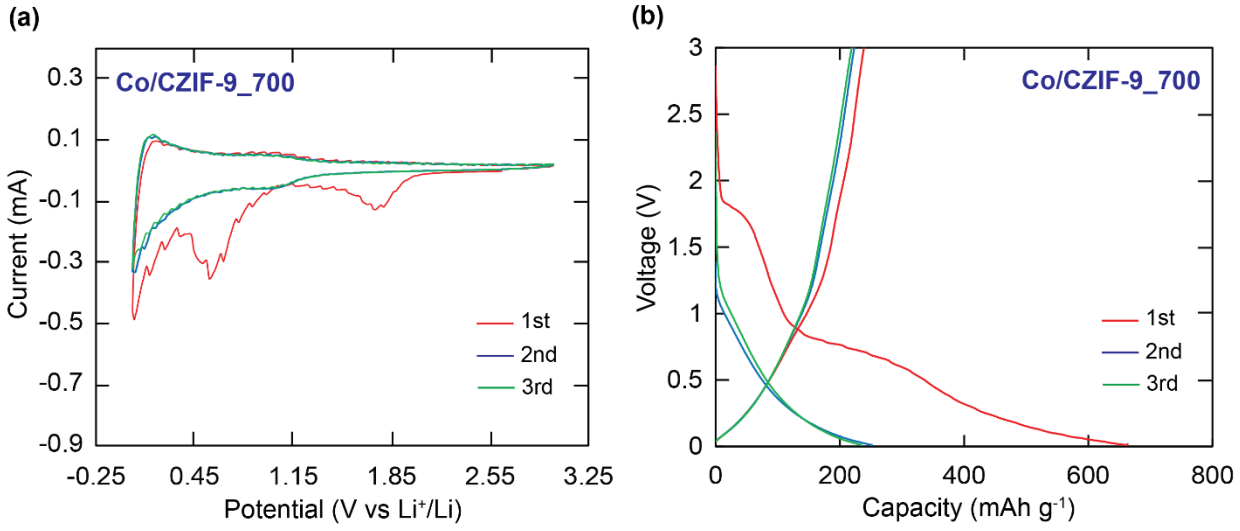

Figure S12. The first three CV curves of Co/CZIF-9_700 at a scan rate of 0.1 mV s^{-1} in the potential range of 0.01-3.0 V (a); The discharge/charge curves of Co/CZIF-9_700 at a current density of 0.1 A g^{-1} for the three cycles (b).

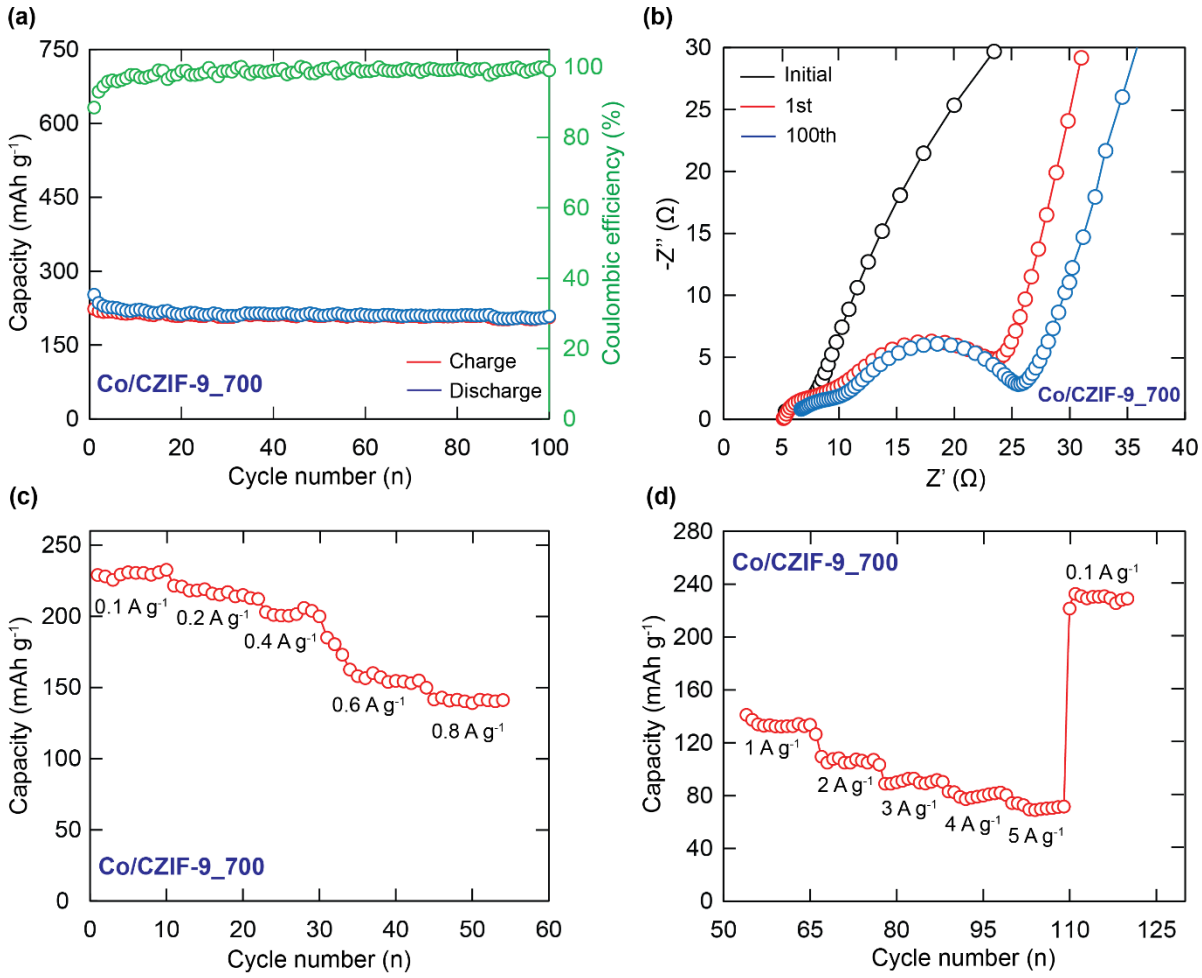

Figure S13. Cycle-life property of Co/CZIF-9_700 at a current density of 0.1 A g^{-1} over 100 cycles (a); The Nyquist plots of Co/CZIF-9_700 material (b); Rate performance of Co/CZIF-9_700 at various current density (c) and (d).

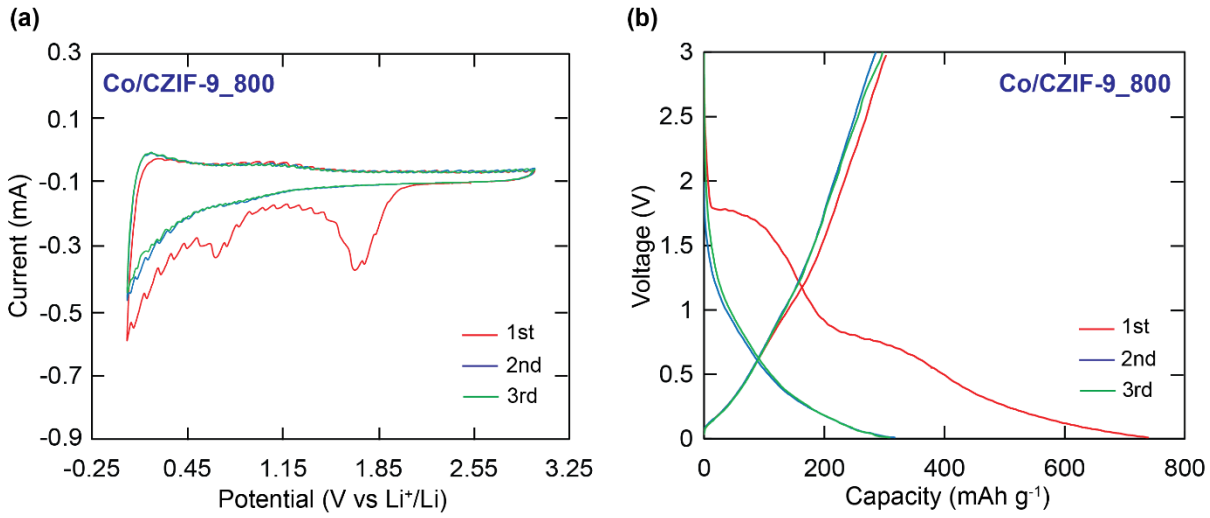

Figure S14. The first three CV curves of Co/CZIF-9_800 at a scan rate of 0.1 mV s^{-1} in the potential range of 0.01-3.0 V (a); The discharge/charge curves of Co/CZIF-9_800 at a current density of 0.1 A g^{-1} for the three cycles (b).

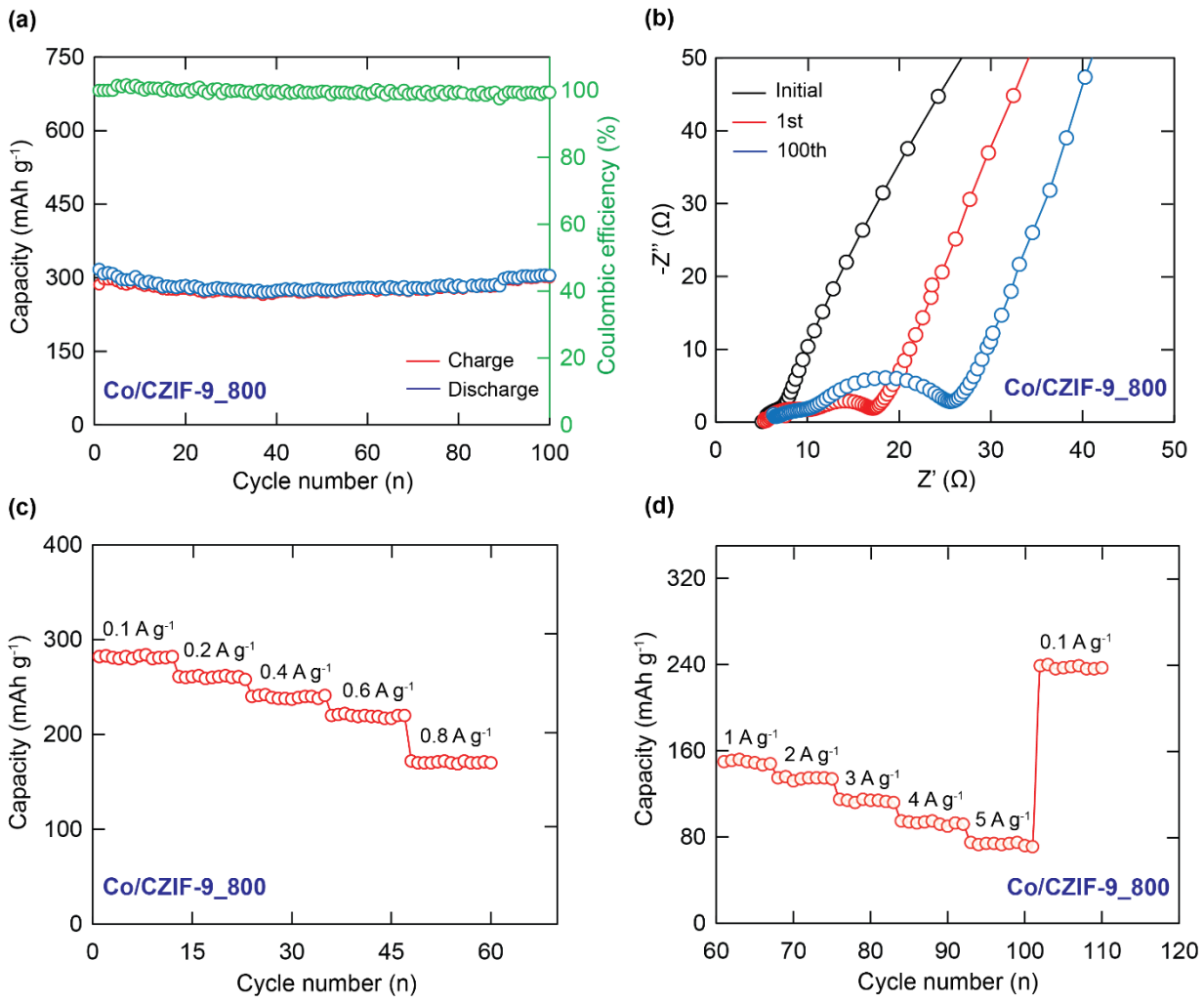

Figure S15. Cycle-life property of Co/CZIF-9_800 at a current density of 0.1 A g^{-1} over 100 cycles (a); The Nyquist plots of Co/CZIF-9_800 material (b); Rate performance of Co/CZIF-9_800 at various current density (c) and (d).

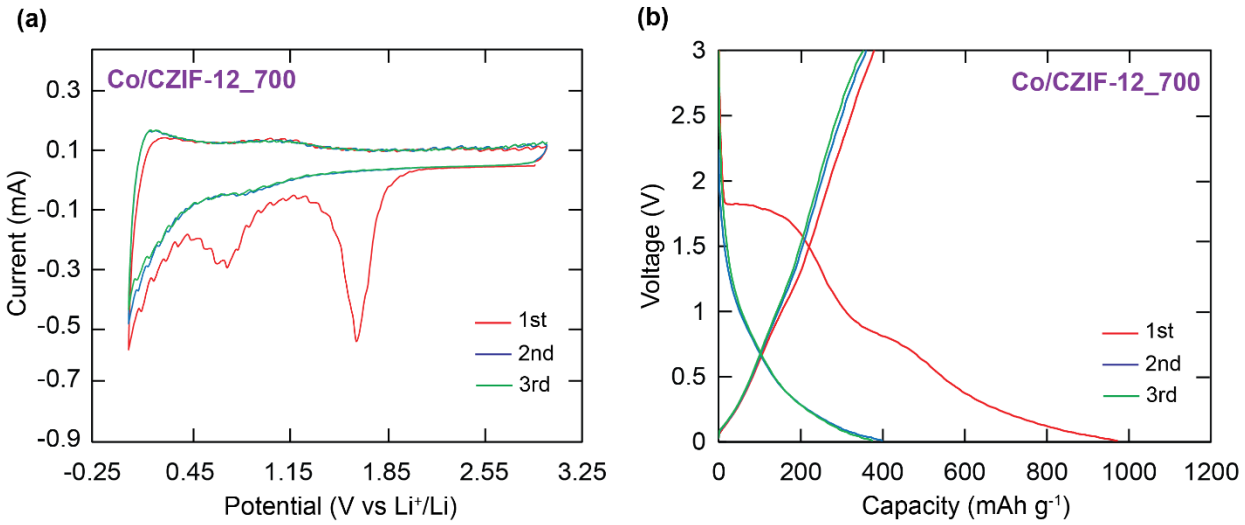

Figure S16. The first three CV curves of Co/CZIF-12_700 at a scan rate of 0.1 mV s^{-1} in the potential range of 0.01-3.0 V (a); The discharge/charge curves of Co/CZIF-12_700 at a current density of 0.1 A g^{-1} for the three cycles (b).

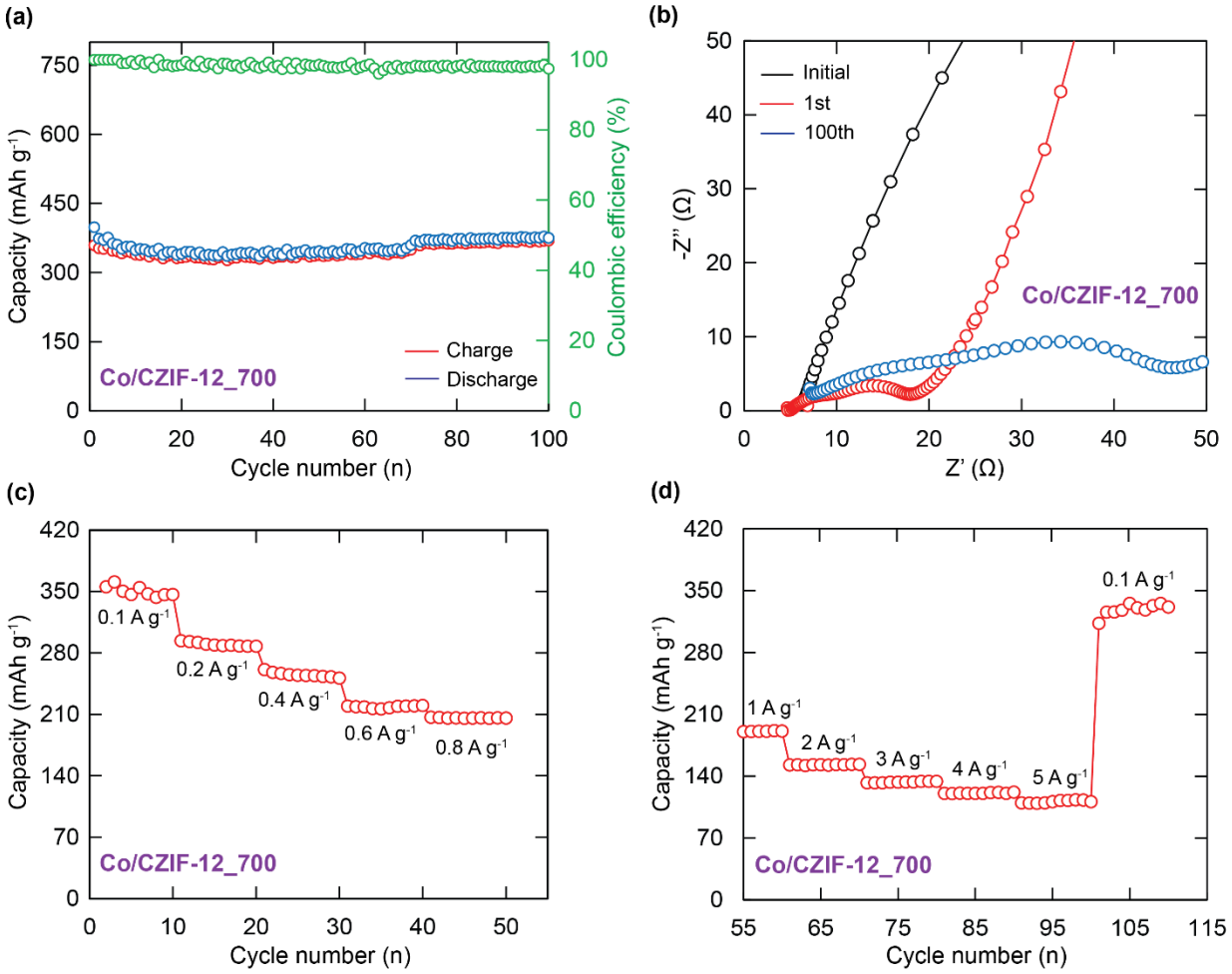

Figure S17. Cycle-life property of Co/CZIF-12_700 at a current density of 0.1 A g^{-1} over 100 cycles (a); The Nyquist plots of Co/CZIF-12_700 material (b); Rate performance of Co/CZIF-12_700 at various current density (c) and (d).

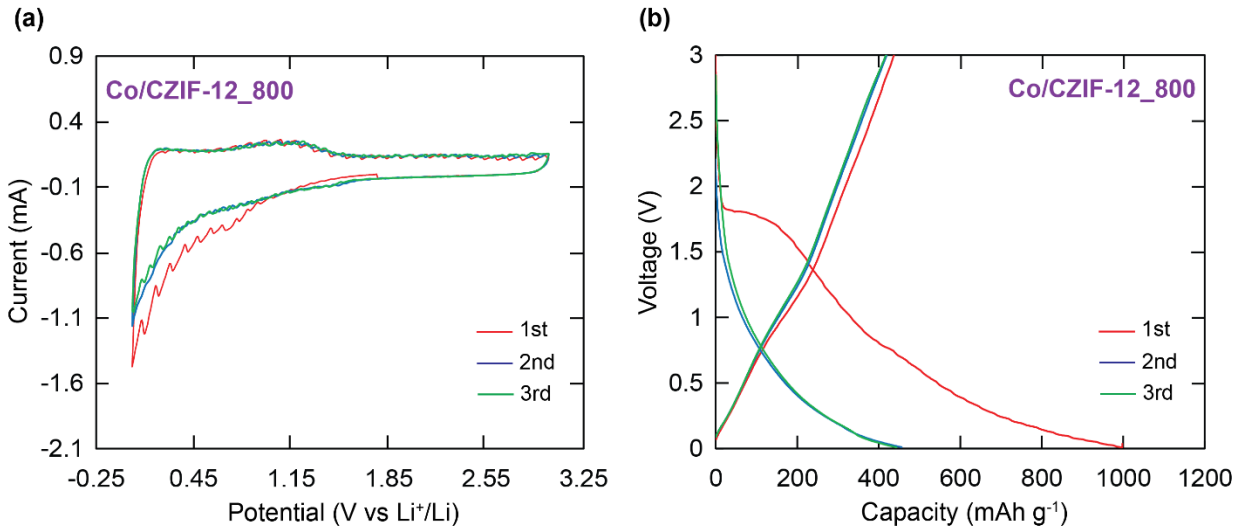

Figure S18. The first three CV curves of Co/CZIF-12_800 at a scan rate of 0.1 mV s^{-1} in the potential range of 0.01-3.0 V (a); The discharge/charge curves of Co/CZIF-12_800 at a current density of 0.1 A g^{-1} for the three cycles (b).

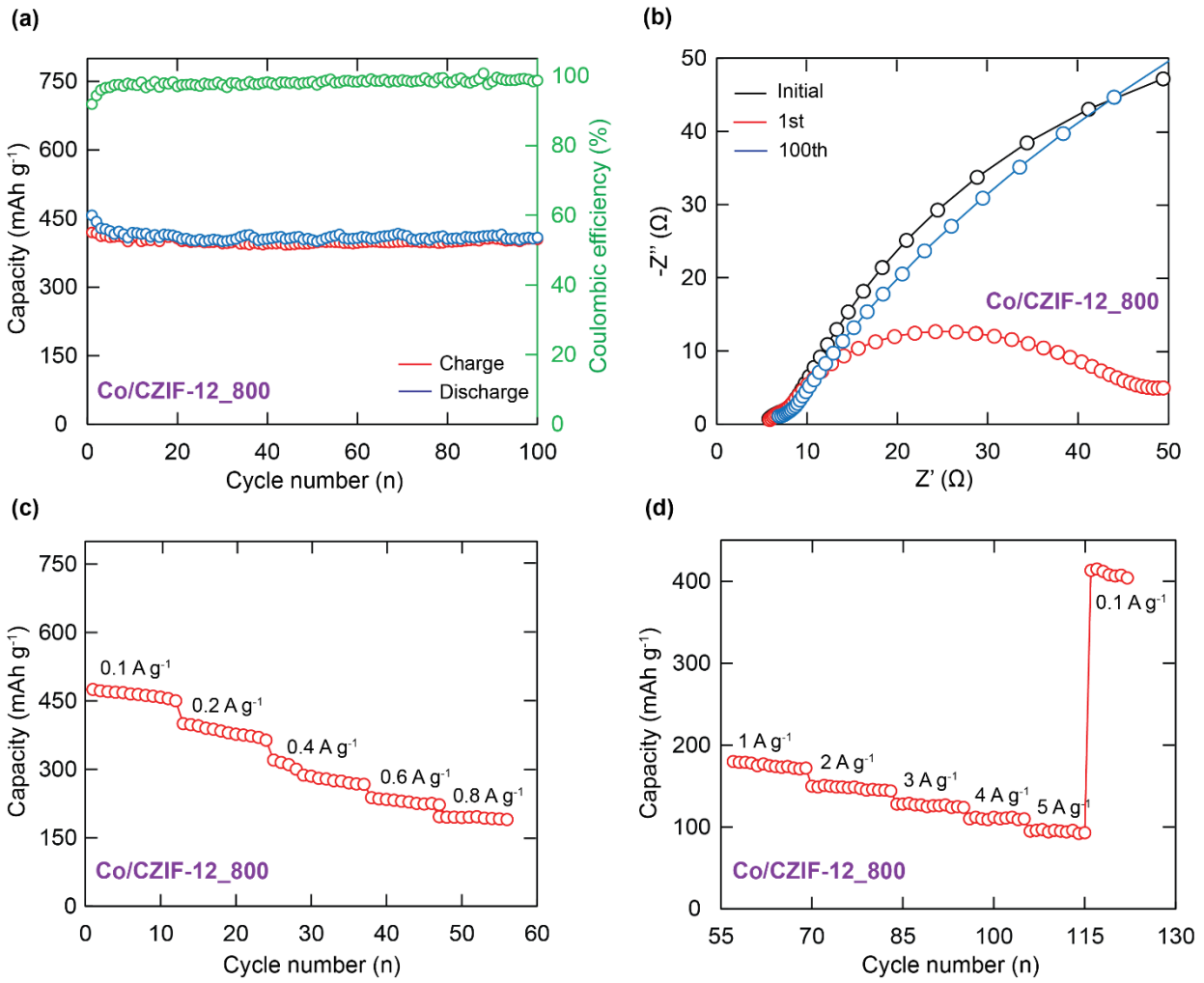

Figure S19. Cycle-life property of Co/CZIF-12_800 at a current density of 0.1 A g^{-1} over 100 cycles (a); The Nyquist plots of Co/CZIF-12_800 material (b); Rate performance of Co/CZIF-12_800 at various current density (c) and (d).